energies

MDPI

Article

Dynamic CO_2 Emission Differences Between E10 and E85 Fuels Based on Speed–Acceleration Mapping

Piotr Laskowski [1,*], Edward Kozłowski [2,*], Magdalena Zimakowska-Laskowska [3], Piotr Wiśniowski [3], Jonas Matijošius [4], Stanisław Oszczak [5], Robertas Keršys [6], Marcin Krzysztof Wojs [1] and Szymon Dowkontt [1]

1 Faculty of Automotive and Construction Machinery Engineering, Warsaw University of Technology, 84 Narbutta Str., 02-524 Warsaw, Poland; marcin.wojs@pw.edu.pl (M.K.W.); szymon.dowkontt@pw.edu.pl (S.D.)
2 Faculty of Management, Lublin University of Technology, 38D Nadbystrzycka Str., 20-618 Lublin, Poland
3 Environment Protection Centre, Motor Transport Institute, 80 Jagiellońska Str., 03-301 Warsaw, Poland; magdalena.zimakowska-laskowska@its.waw.pl (M.Z.-L.); piotr.wisniowski@its.waw.pl (P.W.)
4 Mechanical Science Institute, Vilnius Gediminas Technical University, Plytinės Str. 25, 10105 Vilnius, Lithuania; jonas.matijosius@vilniustech.lt
5 Faculty of Navigation, Polish Air Force University, Dywizjonu 303 Str. 35, 08-521 Dęblin, Poland; oszczak@uni.olsztyn.pl
6 Department of Transport Engineering, Faculty of Mechanical Engineering and Design, Kaunas University of Technology, Studentų Str. 56, LT-51424 Kaunas, Lithuania; robertas.kersys@ktu.lt
* Correspondence: piotr.laskowski@pw.edu.pl (P.L.); e.kozlovski@pollub.pl (E.K.)

Abstract

This study compared CO_2 emissions during a WLTP (Worldwide Harmonized Light-Duty Vehicles Test Procedure) test performed on a chassis dynamometer for the same flex-fuel vehicle, fuelled sequentially with E10 gasoline and E85 fuel. Based on the test data, a CO_2 emissions map was created, describing its dependence on speed and acceleration. The use of a 3D surface enabled the visualisation of the whole dynamics of emissions as a function of engine load in the WLTP cycle, including the identification of distinct emission peaks in areas of high positive acceleration. Analysis of the emission surface enabled the identification of structural differences between the fuels. For E85, more pronounced emission increases are observed in areas of intense acceleration, a consequence of the higher fuel demand resulting from the lower calorific value of bioethanol. In steady-state and moderate-load driving, CO_2 emissions for both fuels are similar. The results confirm that the main differences between E10 and E85 are not simply a shift in emission levels per se, but stem from variations in engine load during the dynamic cycle. Although E85 emits measurable CO_2 emissions, its carbon is not of fossil origin, highlighting the importance of biofuels in the context of greenhouse gas emission reduction strategies and the pursuit of climate neutrality. The presented methodology, combining chassis dynamometer tests with analysis of the speed-acceleration emission map, provides a tool for clearly identifying emission zones and can serve as a basis for further optimisation of engine control strategies and assessing the impact of fuel composition on emissions under dynamic conditions.

Keywords: alcohol fuel; bioethanol; CO_2 emissions; flex-fuel vehicle; internal combustion engine; speed–acceleration map; emission modelling

Academic Editor: Maria Founti

Received: 4 December 2025
Revised: 17 December 2025
Accepted: 18 December 2025
Published: 21 December 2025

1. Introduction

Precisely assessing carbon dioxide emissions under dynamic driving conditions is becoming a key element of contemporary research on drive systems and their environ-

mental impact. With increasingly stringent requirements for reducing greenhouse gas emissions, renewable fuels such as high-percentage bioethanol are gaining importance. Flex-fuel vehicles, capable of running on both E10 gasoline and ethanol blends such as E85, enable direct comparisons of the same drive system's performance with different fuel compositions, eliminating uncertainties related to vehicle design differences.

This paper presents a methodology for comparing CO_2 emissions generated during a WLTP test conducted on a chassis dynamometer for a single flex-fuel vehicle, which is fuelled sequentially with E10 and E85 fuel. The collected data were used to develop two-dimensional and three-dimensional CO_2 emission surfaces in the speed-acceleration system, allowing for the whole dynamics of emissions as a function of engine load. Such emission maps enable the identification of areas with particularly intense emissions, especially during periods of positive acceleration, when energy demand increases rapidly.

The analysis revealed apparent differences between the fuels. In the case of E85, CO_2 emissions exhibit stronger peaks during intense acceleration phases, which is directly related to higher fuel consumption resulting from the lower calorific value of bioethanol. At the same time, under steady state driving conditions and under moderate loads, the emission levels of E10 and E85 are similar. This means that the differences between them are not simply a shift in average emissions but rather result from dynamic variations in engine load during the cycle.

It is worth emphasising that while combustion of E85 also generates carbon dioxide, its carbon is biogenic and does not come from fossil sources. This is important from the perspective of the net emission reduction strategy and the pursuit of climate neutrality. The presented methodology, combining dynamometer data with analysis of speed- and acceleration-dependent emission surfaces, provides a practical tool for assessing the impact of fuel type on emissions under dynamic conditions. It also enables the identification of areas where CO_2 emissions are higher with E85, as well as the detection of differences resulting from the distinct dynamic properties of vehicles fuelled with E10 and E85.

The main objective of this study was to determine the vehicle telemetry regions in which CO_2 emissions increase due to the ethanol content in the fuel, rather than simply comparing general emission characteristics of E10 and E85.

The novelty of this work consists of:

- developing a CO_2 emission model dependent on vehicle speed and acceleration,
- identifying driving zones where CO_2 emissions are higher with E85,
- determining differences in emissions resulting from the driving dynamics of vehicles fueled with E10 and E85.

2. Literature Review

In the literature, bioethanol is presented as a key alternative fuel for spark-ignition engines, capable of reducing greenhouse gas emissions and many toxic pollutants. High-percentage ethanol blends, such as E85 (85% ethanol, 15% gasoline), allow for a moderate reduction in CO_2 emissions from the exhaust system, typically by about 6–9% compared to gasoline under controlled conditions [1]. However, in road tests, this effect is sometimes weaker or statistically insignificant, and its strength depends strongly on the vehicle type and driving conditions [2,3]. This is because the lower carbon content in ethanol is partially compensated by the higher fuel consumption associated with its lower energy density [2]. However, Warguła [4] point out that the change in fuel composition itself (switching from E5 to E10) with suboptimal control of the λ coefficient can lead to non-intuitive changes in exhaust emissions, including an increase in CO_2 and HC while decreasing CO and NOx, even though the engine operating cycle remains unchanged.

Much more pronounced differences emerge in life-cycle analyses (LCAs). Well-to-wheel comparisons indicate that E85 can reduce total GHG emissions by about 43–57% compared to gasoline, with the most significant benefits being achieved for second-generation ethanol produced from lignocellulosic biomass or waste [5]. Corn ethanol provides smaller, but still positive, emission reductions.

Comparisons of E10 vs. E85 blends have shown that E85 typically leads to lower CO_2 emissions (by approximately 6–17%) [2,6]. Studies examining the transition from E5 to E10 have shown that, with proper AFR control, E10 can lead to a slight increase in CO_2 and NOx emissions, while decreasing CO and HC emissions. However, with improper λ calibration, additional emission deviations occur [4].

Similar conclusions are drawn from broader analyses of bioethanol as a fuel. E10–E85 blends typically result in a slight increase in tailpipe CO_2 emissions due to more complete combustion, which, however, is compensated at the life-cycle level by the biogenic origin of the carbon [7,8]. The environmental balance of bioethanol is strongly dependent on the type of feedstock, production technology, and impacts on categories such as acidification and eutrophication [9,10].

For flex-fuel vehicles (FFVs), road studies in Brazil and Asia indicate that increasing the share of ethanol in the fuel typically reduces CO_2 emissions per kilometre and emissions of many regulated pollutants, at the expense of increased fuel consumption [3,6,11,12]. Well-to-wheel analyses indicate that primary ethanol can reduce CO_2 emissions by approximately 58% compared to gasoline, and second-generation ethanol by up to 73% [13,14].

The introduction of the global WLTP procedure was intended to make vehicle emissions assessments more realistic than the previous NEDC cycle. These changes include higher test masses, more realistic rolling resistance coefficients, and a more dynamic speed and acceleration profile, which translates into higher reported CO_2 emissions [15]. On average, CO_2 emissions measured in the WLTP are approximately 21–25% higher for passenger cars and approximately 27% higher for commercial vehicles than in the NEDC, with this powerful effect on diesel vehicles and classic hybrids [16].

The application of the WLTP to ethanol blends shows that high ethanol (E75/E85) content allows for an additional reduction in NOx emissions by up to 30–55% and, in some studies, also CO_2 emissions, but at the same time significantly increases the emissions of CO, methane, aldehydes (especially acetaldehyde), and unburned ethanol, especially at low temperatures and during the cold start phase [17–20]. Emissions of these compounds under WLTP conditions are generally higher than in older cycles.

Chassis dynamometer testing remains a key tool for assessing CO_2 emissions, ensuring high measurement repeatability and facilitating comparisons between vehicles. At the same time, numerous studies indicate that laboratory emission values, especially those based on older cycles, underestimate real-world emissions on the road by an average of 9–23% [21–23]. The magnitude of the error depends on the cycle used, the dynamometer load settings, and the vehicle type and fuel [17,24,25]. Similar conclusions were obtained by Kuranc [26], who compared the emissions of selected exhaust gas components and fuel consumption of the same passenger car in different driving cycles on a chassis dynamometer, demonstrating significant sensitivity of the results to the shape of the speed profile and driving dynamics.

The literature emphasises that dynamic driving cycles, both standard (WLTC) and local, better reflect real-world emissions; however, they still do not fully reproduce aggressive acceleration, urban traffic conditions (stop-and-go), or the impact of weather conditions. Hence, the growing importance of RDE studies using PEMS and predictive models calibrated on field data [21,27,28].

Modern CO_2 emission models are shifting away from the average speed approach toward microscopic models that utilise instantaneous speed, acceleration, vehicle-specific power (VSP), and road slope. These models are built on both physical equations that describe energy balance and vehicle dynamics, as well as advanced machine learning methods [29–32].

Models based on neural networks (MLP, LSTM), random forest or hybrid models achieve very high accuracy (R^2 0.98) in the prediction of instantaneous emissions, better than classical regression models in reproducing the nonlinear and transient behaviour of the drive system [28,33–35]. The use of speed-acceleration-emission maps enables visualisation and quantitative assessment of the areas of space (v, a) where emissions are highest, typically in the case of high speed combined with positive acceleration, while during braking and steady driving, emissions are much lower [36–38].

Emission surface models and structural models are being developed in parallel, combining a microscopic approach with high-resolution spatial grids. These models enable the mapping of emission distributions within the street network and their correlation with traffic volume, fleet structure, and building characteristics [39–41]. Many studies utilise explainable AI techniques (e.g., SHAP) to assess the significance of individual variables and detect structural asymmetries between different vehicle types [42,43].

A key conclusion from these studies is that acceleration and driving dynamics are as important as speed in determining CO_2 emissions, and differences in driving style can modify emissions by up to several to a dozen or so percent for the exact vehicle and route [32,44].

Quantitative analyses of CO_2 emissions indicate a strong relationship between engine load and carbon dioxide emissions. In both spark-ignition and compression-ignition engines, increasing load results in increased fuel consumption and more complete combustion, leading to higher CO_2 concentrations [45–47]. For example, in a diesel marine engine, the CO_2 concentration increased from 2.44% at 30% load to 3.57% at 90% load [45], and in heavy road vehicles, full load at low speeds caused up to a 96% increase in specific CO_2 emissions compared to the unladen vehicle [47].

At the same time, the use of alternative fuels and dual-fuel systems (e.g., hydrogen–methane, hydrogen–diesel, ammonia–diesel) enables significant reductions in CO_2 emissions at high loads. Reductions of 12–65% have been reported for hythane, hydrogen blends, and ammonia/diesel systems, among others [48–51]. Further reductions can be achieved by optimising engine operating parameters, such as injection angle and oil viscosity [52,53]. In parallel to these fuel blends and dual-fuel concepts, novel propulsion systems such as compressed-air engines are being investigated as locally zero-CO_2 alternatives to conventional combustion engines [54].

At the atmospheric scale, attention is drawn to transient spikes in CO_2 concentrations, recorded in high-resolution time series. These spikes are typically the result of local emission events, road traffic, industrial processes, or building heating, and can distort the analysis of long-term trends if not correctly identified and filtered [55–57].

The development of instantaneous CO_2 emission models, using machine learning, time series, and dispersion models, enables very accurate (R^2 up to 0.99) emission predictions on a second-to-second scale for vehicles, stationary installations, and at the national level [58,59]. The use of OBD, PEMS, and IoT sensor data also enables real-time emission estimation for individual vehicles and fleets, which forms the basis for eco-driving and traffic management systems [60–62].

Studies on the variability of CO_2 emissions show that for vehicles with similar parameters, emissions can vary by as much as 50% or more depending on driving style, traffic conditions, terrain, ambient temperature, and vehicle age and type [63–66]. This

highlights the need for models and measurement procedures that account for real-world operating conditions.

In the context of climate policy, it is important to distinguish between fossil and biogenic CO_2 emissions. Bioethanol, biodiesel, biomethane, and other biofuels recycle carbon previously sequestered in biomass, which is the basis for considering their emissions as potentially "carbon neutral." In practice, however, this balance depends on the entire fuel life cycle, including land-use changes, energy inputs, and process emissions [67,68].

LCAs indicate that first-generation biofuels (e.g., corn ethanol, vegetable oil biodiesel) rarely achieve complete carbon neutrality; one study estimated that biogenic CO_2 absorption offsets only about 37% of combustion-related emissions [69]. A better balance is achieved for biofuels derived from waste and lignocellulosic feedstocks, as well as for systems integrated with CO_2 capture and storage (BECCS), which can mitigate harmful emissions [70–72].

Measurements and modelling are being conducted in cities to separate fossil and biogenic CO_2 fluxes. Results suggest that while urban vegetation can partially offset transport emissions during the growing season, most metropolitan areas remain a net source of CO_2 due to high traffic volumes and limited green space [73–75].

At the fuel level, detailed analyses of the ethanol carbon cycle reveal a broad spectrum of emission intensities, ranging from moderate reductions for classic corn ethanol to potentially harmful emissions for lignocellulosic ethanol utilising CCS and renewable energy [76,77]. In turn, comprehensive LCAs of bioethanol emphasise the role of feedstock selection, process solutions, and allocation methods in shaping the resulting GHG indicators, as well as the potential for increases in other impact categories, such as acidification and eutrophication [78,79].

From a broader perspective, renewable fuels, both biofuels and synthetic fuels produced using renewable energy, play a significant role in reducing CO_2 emissions in the transport and energy sectors. However, the scale of the effect varies significantly across regions and depends on the technology mix, renewable energy penetration level, and supporting policies [80,81].

Recent research increasingly highlights that cycle-averaged CO_2 indicators can mask substantial load-dependent variability. Consequently, instantaneous emission modelling approaches based on speed, acceleration, and related proxies (e.g., VSP), as well as machine learning techniques, have been intensively developed to capture transient behaviour and improve prediction accuracy [29,31–33,39–41,44,58,82,83]. In parallel, studies investigating ethanol–gasoline blends, including high-ethanol fuels, report that emission responses depend strongly on driving conditions (e.g., urban vs. rural operation, cold-start effects, and on-road vs. laboratory testing) rather than solely on ethanol content [1–3,6,12,13,18,84,85]. These findings motivate the present work, which combines WLTP chassis dynamometer testing with speed–acceleration emission mapping and a differential index to localise fuel-dependent CO_2 differences in the operating-state space.

3. Materials and Methods

The test was conducted on a chassis dynamometer using a flex-fuel vehicle designed to run on both E10 gasoline and E85 ethanol fuel. The exact vehicle was subjected to the complete WLTP procedure, repeating the cycle three times for each fuel, under identical load, temperature, and dynamometer settings. This eliminates variability resulting from differences in vehicle design or operation, and any differences in emissions can be attributed to variations in fuel composition and changes in driving dynamics.

Figure 1 shows an example of a vehicle's speed curve during the WLTP test, along with the designation of each phase of the cycle. The instantaneous acceleration value was determined from the speed signal, allowing for a complete description of the driving dynamics.

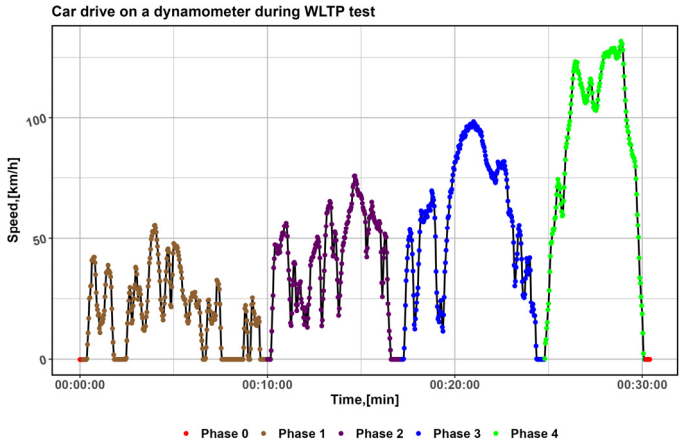

Figure 1. Vehicle speed profile and WLTP phases during the chassis dynamometer test.

Although the target WLTP speed profile is identical for both fuels, slight differences in instantaneous speed and acceleration are inevitable in physical chassis dynamometer tests. They may arise from fuel-dependent drivetrain responses and control strategies. These differences are reflected in the speed–acceleration distributions shown in Figure 2.

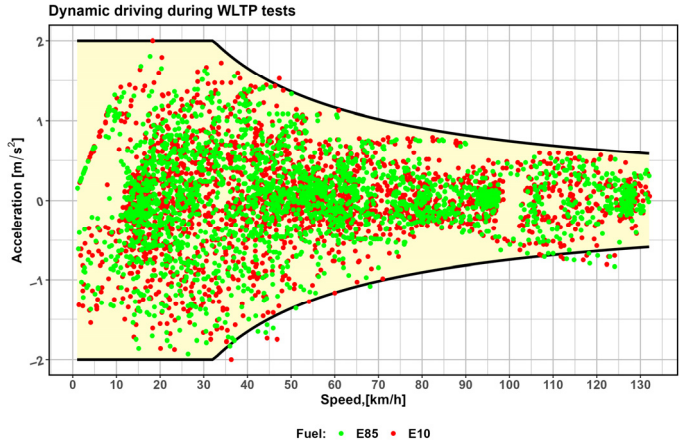

Figure 2. Speed–acceleration distribution during WLTP tests for E10 and E85 fuels.

To compare pollutant emissions, vehicle speed [km/h], acceleration [m/s^2] and pollutant value [g/km] were analysed. Let $\{(t_i, V_i^c, P_i^c)\}_{0 \le i \le n^c}$ be a sequence of readings during a drive on the dynamometer, where V_i^c denotes the vehicle speed [km/h] when the engine was powered by fuel $c \in \{E10, E85\}$, P_i^c—emission [g/km] at $i-$th moment, $0 \le i \le n^c$. The WLTP test has been repeated 3 times ($j \in \{1, 2, 3\}$) for each fuel. Figure 1 shows the example of speed readings (black line) during the tests. In addition, on Figure 1 at each moment the phases have been marked. To estimate the impact of vehicle dynamics on emissions, we analyse acceleration in addition to speed. Thus for the test we create data set $\{(V_i^c, a_i^c, P_i^c)\}_{0 \le i \le n_j^c}$, where $a_i^c = \frac{1000(V_i^c - V_{i-1}^c)}{(t_i - t_{i-1})3600}$ for $1 \le i \le n^c$ and $a_i^c = 0$ for fuel $c \in \{E10, E85\}$. We only analyse vehicles in motion, so we select readings from the data set for which the speed exceeds 1 [km/h].

4. Analysis of Emission During Tests

Let $\{(V_t, a_t, P_t)\}_{1\leq t\leq n}$ denotes the data set containing speed, acceleration and instantaneous pollution. The main task is to identify the relationship between pollution and vehicle speed and acceleration, and thus to determine $P_t = f(\Theta, V_t, a_t, \varepsilon_t)$, where $\{\varepsilon_t\}_{1\leq t\leq n}$ denotes a sequence of independent identically distributed random variables with normal distribution $N(0, \sigma^2)$ and Θ—model parameters. Detailed models of the engine operating cycle, describing the energy balance, thermodynamic changes in the cylinder, and the dependence of emissions on load, are widely discussed in the literature on modelling combustion engines [86]. However, in this work, a simplified, empirical approach was used, which allows for direct identification of the relationship based on data from a chassis dynamometer.

The impact of vehicle dynamics on pollution is defined as follows

$$P_t = CV_t^{\theta_1+\theta_2 a_t} e^{\theta_3 V_t+\theta_4 a_t+\theta_5 V_t a_t+\theta_6 V_t^2+\theta_7 a_t^2+\varepsilon_t} \tag{1}$$

Because we analyse pollution generated by the vehicle in motion, then $P_t > 0$ for $1 \leq t \leq n$, thus Equation (1) can be presented as follows

$$\log(P_t) = \theta_0 + \theta_1 \log(V_t) + \theta_2 a_t \log(V_t) + \theta_3 V_t + \theta_4 a_t + \theta_5 V_t a_t + \theta_6 V_t^2 + \theta_7 a_t^2 + \varepsilon_t \tag{2}$$

where $C = e^{\theta_0}$. To estimate the unknown parameters in (2) we use Ordinary Least Square Method [87,88]. Thus we define the matrices

$$X = \begin{bmatrix} 1 & \log(V_1) & a_1\log(V_1) & V_1 & a_1 & V_1 a_1 & V_1^2 & a_1^2 \\ 1 & \log(V_2) & a_2\log(V_2) & V_2 & a_2 & V_2 a_2 & V_2^2 & a_2^2 \\ \vdots & \vdots & \vdots & \vdots & \vdots & \vdots & \vdots & \vdots \\ 1 & \log(V_n) & a_n\log(V_n) & V_n & a_n & V_n a_n & V_n^2 & a_n^2 \end{bmatrix}, \quad Y = \begin{bmatrix} \log(P_1) \\ \log(P_2) \\ \vdots \\ \log(P_n) \end{bmatrix}, \quad \Theta = \begin{bmatrix} \theta_0 \\ \theta_1 \\ \vdots \\ \theta_7 \end{bmatrix}, \quad \varepsilon = \begin{bmatrix} \varepsilon_0 \\ \varepsilon_1 \\ \vdots \\ \varepsilon_n \end{bmatrix}$$

In view of the above, we present Equation (2) in linear form

$$Y = X\Theta + \varepsilon \tag{3}$$

To estimate unknown parameters Θ we solve the task [87–89]

$$\min_{\theta} ||Y - X\theta||^2$$

where $||Y - X\theta||^2 = < Y - X\theta, Y - X\theta >$, $< ., .$ denotes dot (scalar) product. From Gauss-Markov theorem if $\det(X^T X) \neq 0$, then Best Linear Unbiased Estimator [82] is given as follows

$$\hat{\Theta} = \left(X^T X\right)^{-1} X^T Y \tag{4}$$

We estimate the prediction of instantaneous pollution based on speed and acceleration on a logarithmic scale as

$$\log(\hat{P}_t) = \hat{\theta}_0 + \hat{\theta}_1 \log(V_t) + \hat{\theta}_2 a_t \log(V_t) + \hat{\theta}_3 V_t + \hat{\theta}_4 a_t + \hat{\theta}_5 V_t a_t + \hat{\theta}_6 V_t^2 + \hat{\theta}_7 a_t^2 \tag{5}$$

The value $\varepsilon_t = \log(P_t) - \log(\hat{P}_t) = \log\left(\frac{P_t}{\hat{P}_t}\right)$ denotes differences between empirical and predicted values of instantaneous pollution on a logarithmic scale $1 \leq t \leq n$ and $\varepsilon = (\varepsilon_1, \varepsilon_2, \ldots, \varepsilon_n)$ denotes the residual vector according to model (2), but variance of residuals is equal $\sigma^2 = \frac{\varepsilon^T \varepsilon}{n-8}$. The vector of variance of structural parameters we estimate as $\left(S_{\theta_0}^2, S_{\theta_1}^2, \ldots, S_{\theta_7}^2\right) = \sigma^2 diag\left(\left(X^T X\right)^{-1}\right)$.

To assess the impact of velocity, acceleration and the transformation of these variables on instantaneous pollution at a significance level of $0 < \alpha < 1$ for each, parameter we create a null hypothesis [87,88,90]:

H_0: $\theta_i^s = 0$ *(the influence of the i-th factor is insignificant on the instantaneous pollution)*

and alternative hypothesis

H_1: $\theta_i^s \neq 0$ *(the i-th factor significant influences on the instantaneous pollution).*

The statistic

$$T_i = \frac{\hat{\theta}_i^s}{S_{\theta_i}} \sqrt{n-8} \tag{6}$$

has t-distribution with $(k-8)$ degrees of freedom. For each parameter the test probability (p-value) is equal.

$$p_i = 2 * P(T > |T_i|),$$

where T random variable t-distribution with $(n-8)$ degrees of freedom, $i \in \{0, 1, \ldots, 7\}$. If for $i-$th parameter the inequality $p_i \geq \alpha$ is satisfied, then at the significance level α there is no basis to reject the null hypothesis, thus $i-$th structural parameter is insignificantly different from zero, and the corresponding predictor has a nonsignificant effect on explaining the variability of instantaneous pollution. If $p_i < \alpha$, then at the significance level α, we reject the null hypothesis H_0 in favour of the alternative hypothesis, then the structural parameter is significantly different from zero, and the corresponding predictor significantly impacts the explanation of instantaneous pollution variability.

Determination coefficient shows what part of the variability of the transformed variable is explained by the model and is estimated as

$$R^2 = 1 - \frac{\sum_{t=1}^{n} \left(\log(P_t) - \log(\hat{P}_t)\right)^2}{\sum_{t=1}^{n} \left(\log(P_t) - \bar{P}\right)^2} \tag{7}$$

where $\bar{P} = \frac{1}{n} \sum_{t=1}^{n} \log(P_t)$.

To evaluate how well the model fits the empirical data, we assess the significance of the multiple correlation coefficient. For this purpose, at significance level of $0 < \alpha < 1$ we create a null hypothesis:

H_0: $R = 0$ *(multiple correlation coefficient is insignificant, the model does not explain well variability of instantaneous pollution)*

and alternative hypothesis

H_1: $R \neq 0$ *(the model explain quite well variability of instantaneous pollution)*

For model (2) the test statistics is equal

$$h = \frac{R^2}{1-R^2} * \frac{n-7-1}{7} \tag{8}$$

and test probability $p_{val} = P(F > h)$, where F random variable has a Fisher-Snedecor distribution with $(7, n-8)$ degrees of freedom. If $p_{val} \geq \alpha$, then there is no reason to reject the null hypothesis, thus the multiple correlation coefficient is insignificantly different from 0 and the fit of model to the data is quite weak. If $p_{val} < \alpha$, we reject the null hypothesis H_0 in favour of alternative hypothesis H_1, thus the fit of the model to the data is sufficiently high, and the model can be used for forecasting instantaneous pollution.

5. Results

To examine the driving load on instantaneous CO_2 emissions, the first instance of a speed and acceleration curve during the WLTP cycle was analysed. Figure 2 illustrates the full vehicle motion signal obtained from a chassis dynamometer. These data were used to determine predictors in the regression model and to construct emission maps in the speed-acceleration space.

Figure 2 shows the velocity space and the corresponding acceleration values obtained during WLTP runs performed on a chassis dynamometer for both fuel types. Green points indicate observations for E85 fuel, while red points indicate observations for E10. The area of permissible acceleration is defined by black limiting curves, between which all recorded instantaneous values lie.

In the case of a run for different fuels, we analyse the speed and acceleration area $\left\{(V_t, a_t) : 1 \leq V_t \leq 132, \max\left(-2, -41 * V_t^{-0.87}\right) \leq a_t \leq \min\left(2, 41 * V_t^{-0.87}\right), 1 \leq t \leq n\right\}$ (the acceleration value is between the curves marked in black). For each fuel, we identify the effect of speed and acceleration on instantaneous emissions, thus identifying the structural parameters $\theta_0^{E10}, \theta_1^{E10}, \ldots, \theta_7^{E10}$ for E10 and $\theta_0^{E85}, \theta_1^{E85}, \ldots, \theta_7^{E85}$ for E85. As a prediction of pollution for the area $\{(V, a) : -2 \leq a \leq 2, 1 \leq V \leq 132\}$ we determine

$$P_c(V,a) = \begin{cases} g(V,a,c), & 1 \leq V \leq 132, \quad \max\left(-2, -41 * V^{-0.87}\right) \leq a \leq \min\left(2, 41 * V^{-0.87}\right) \\ 0, & \text{other} \end{cases} \tag{9}$$

where $g(V,a,c) = V^{\theta_1^c + \theta_2^c a} e^{\theta_0^c + \theta_3^c V + \theta_4^c a + \theta_5^c Va + \theta_6^c V^2 + \theta_7^c a^2}$ for $c \in \{E10, E85\}$.

In the first stage of the analysis, the parameters of model (2) were estimated for the runs using E10 fuel. The values of the structural coefficients, their standard errors, and Student's t-statistics and the corresponding p-values are presented in Table 1. The model describes the dependence of instantaneous emissions on speed and acceleration, as well as the transformation of these variables on a logarithmic scale.

Table 1. Parameters of the model of instantaneous pollution in logarithmic scale for the vehicle powered by E10 fuel.

	θ_j^{E10}	$S_{\theta_j^{E10}}$	t_j	p_j
j = 0	7.77974	0.11166	69.67153	0
j = 1	−0.90216	0.05313	−16.98035	4.8133×10^{-61}
j = 2	0.10142	0.04486	2.26088	0.02386
j = 3	0.00764	0.0027	2.83167	0.00467
j = 4	0.20812	0.11319	1.8386	0.0661
j = 5	0.0036	0.00132	2.72613	0.00646
j = 6	0.00004719	1.3204×10^{-5}	3.5734	0.00036
j = 7	0.12972	0.0161	8.05862	1.2223×10^{-15}

Analysing the influence of predictors (speed, acceleration, and transformations of these predictors), we see that at a significance level of 0.05, there is no basis to reject the working hypothesis for the structural parameter θ_4^{E10} (acceleration a_t has a negligible direct effect on pollution). In contrast, the predictors: logarithm of speed, product of acceleration and logarithms of speed, speed, product of acceleration and speed, square of speed and square of acceleration ($\log(V_t), a_t \log(V_t), V_t, V_t a_t, V_t^2, a_t^2$) have a significant influence on instantaneous emission. The value of the coefficient of determination R^2 2 for model (2) is 0.641. Analyzing the multiple correlation coefficient from formula (8), the value of the test statistic is 591.4471 for (7.2319) degrees of freedom, while the test probability is below

2.2×10^{-16}. This means that the model is well fitted to the empirical data and can be used for further comparative analysis with E85 fuel.

To illustrate the obtained dependencies, Figure 3 presents the surface of predicted instantaneous CO_2 emissions for E10 fuel as a function of speed and acceleration.

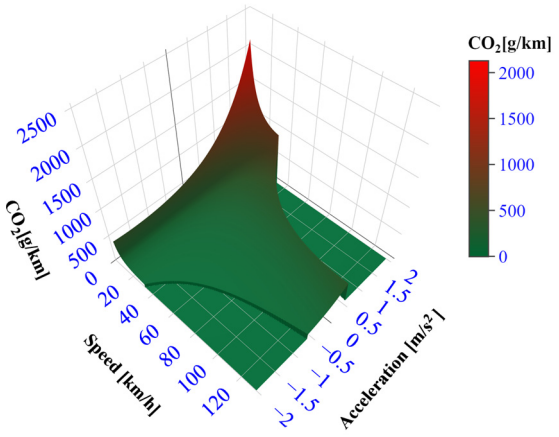

Figure 3. Instantaneous CO_2 emission surface for E10.

Figure 3 shows a three-dimensional surface of instantaneous CO_2 emissions determined based on a model developed for E10 fuel. The highest emission values are observed in the area of positive acceleration and at higher speeds, reflecting increased engine load during intense acceleration phases. As speed increases, acceleration has a decreasing effect on emissions, and the surface becomes flatter, indicating stabilisation of energy demand during steady-state driving. Negative accelerations (braking) and slight positive accelerations at low speeds are characterised by the lowest emission levels, which is typical for spark-ignition engines under low load conditions.

In the next step, the parameters of model (2) were estimated for the trip made using E85 fuel. The obtained values of structural coefficients along with standard errors, Student's t-statistics and the corresponding *p*-values are presented in Table 2.

Table 2. Parameters of the model of instantaneous pollution in logarithmic scale for the vehicle powered by E85 fuel.

	θ_j^{E85}	$S_{\theta_j^{E85}}$	t_j	p_j
j = 0	7.73088	0.09175	84.26171	0
j = 1	−0.903	0.04446	−20.30846	1.5451×10^{-84}
j = 2	0.00039	0.0458	0.00848	0.99323
j = 3	0.00762	0.00237	3.21284	0.00133
j = 4	0.42347	0.11549	3.66674	0.00025
j = 5	0.00988	0.00135	7.2993	3.9524×10^{-13}
j = 6	4.8251×10^{-5}	1.1938×10^{-5}	4.04169	5.4793×10^{-5}
j = 7	0.1065	0.01603	6.64491	3.7675×10^{-11}

Analysing the influence of predictors (speed, acceleration and transformations of these predictors) we see that at the significance level of 0.05 there is no basis to reject the working hypothesis for the structural parameter θ_2^{E85} (the product of acceleration and the logarithm of velocity $a_t \log(V_t)$ directly has a negligible effect on pollution). In contrast, the predictors of the logarithm of velocity, velocity, acceleration, the product of acceleration and velocity, the square of velocity and the square of acceleration $\left(\log(V_t), V_t, a_t, V_t a_t, V_t^2, a_t^2\right)$ have a significant influence on instantaneous emissions. The value of the coefficient of determination R^2 2 for model (2) is 0.6919. Analysing the multiple correlation coefficient

from Formula (8), the test statistic value is 745.413 for (7, 2323) degrees of freedom, while the test probability is below 2.2×10^{-16}, so the model fits the empirical data quite well. These results enable a direct comparison of the emission structures for both fuels and further analysis of the differences in predicting the CO_2 emission surface in the velocity–acceleration space.

To illustrate the obtained relationships for E85 fuel, Figure 4 presents a three-dimensional surface of instantaneous CO_2 emission as a function of speed and acceleration.

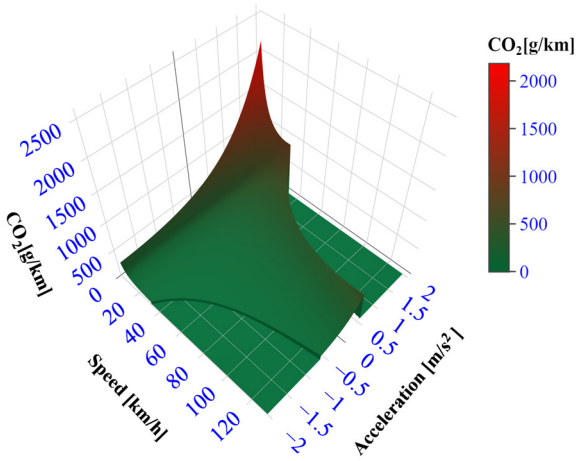

Figure 4. Instantaneous CO_2 emission surface for E85.

Figure 4 illustrates the three-dimensional surface of predicted CO_2 emissions for E85 fuel, derived from the estimated regression model. Compared to E10 fuel, a more pronounced increase in emissions is observed in the region of positive acceleration, especially at higher vehicle speeds. The sharp increase in the surface at the top of the graph reflects the increased energy demand during intense acceleration, which is more pronounced in the case of E85 due to the lower calorific value of ethanol and the need for a larger fuel supply.

At low speeds and under braking, emissions remain low. In the medium speed region, the surface shows a gradual increase with acceleration, similar to E10, but with a larger amplitude. This characteristic indicates a greater sensitivity of instantaneous CO_2 emissions to engine load when using E85 fuel.

To determine the areas with increased/reduced CO_2 emissions due to the ethanol content in the fuel, we determine the coefficient

$$H(V,a) = \begin{cases} \frac{P_{E85}(V,a) - P_{E10}(V,a)}{P_{E10}(V,a)} 100\%, & 1 \le V \le 132, \max\left(-2, -41 * V^{-0.87}\right) \le a \le \min\left(2, 41 * V^{-0.87}\right) \\ 0, & \text{other} \end{cases} \quad (10)$$

for the entire area $\{(V,a) : -2 \le a \le 2, 1 \le V \le 132\}$.

The coefficient $H(V,a)$ shows the percentage increase or decrease in CO_2 emissions for E85 fuel compared to E10 fuel. To illustrate the differences in CO_2 emissions between fuels across the entire speed and acceleration range, the values of the coefficient $H(V,a)$ are reproduced in Figure 5.

Figure 5 shows the percentage difference between CO_2 emissions predicted for E85 and those determined for E10. Red indicates areas where E85 generates higher emissions, while green indicates a reduction in emissions relative to E10. The most significant emission increases are observed in the positive acceleration zone, especially at speeds above approximately 40 km/h, which corresponds to phases of in-tense engine load. In the low-speed and negative acceleration zones, the differences remain small or negative, indicating that under light-load conditions, E85 does not increase CO_2 emissions relative to E10.

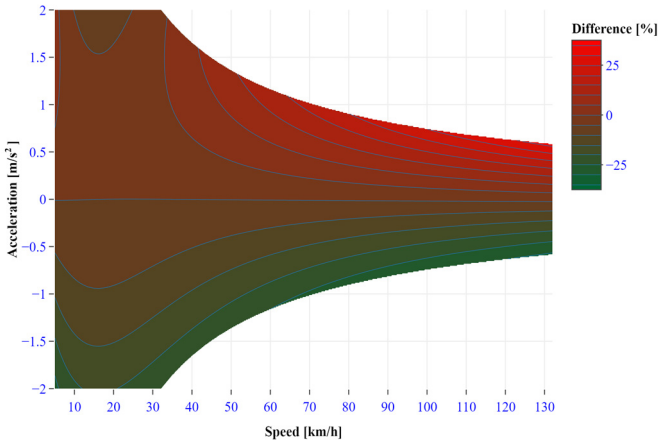

Figure 5. Percentage difference in predicted CO_2 emissions for E85 relative to E10 across the speed–acceleration domain.

The shape of the map reveals a clear causal link between vehicle dynamics, engine operating conditions and the relative CO_2 performance of both fuels. At higher positive accelerations the engine must rapidly increase torque, which for E85 requires a noticeably larger mass of fuel because of its lower-heating value. Under these conditions the stoichiometric advantage of ethanol (higher oxygen content and potential for more efficient combustion) is not sufficient to offset the increased fuel mass, so the net tailpipe CO_2 per unit distance becomes higher than for E10. As speed rises, these high-load events become longer and more energy intensive, which explains the broad red region at medium and high speeds. Conversely, in the negative acceleration region, the throttle is mostly closed, and, at stronger decelerations, fuel cut-off is often activated. Here the influence of the fuel type on instantaneous CO_2 becomes marginal, and small calibration differences may even favour E85, leading to the slightly green areas. Around zero acceleration, especially at moderate and higher speeds, the differences tend towards zero, reflecting steady cruising where both fuels operate near similar indicated efficiency and the engine control system converges to comparable air–fuel and ignition settings. Overall, the map indicates that the impact of switching from E10 to E85 is strongly load-dependent: aggressive, acceleration-dominated driving tends to amplify CO_2 differences to the disadvantage of E85, whereas smoother, low-load operation largely neutralizes them.

Using the $H(V,a)$ value defined in (11), we determine the areas of vehicle dynamics (speed and acceleration) for which we see a clear increase in emissions, as well as areas of emission reduction caused by adding more ethanol to the fuel. Figure 6 clearly shows that E85 fuel generates higher CO_2 emissions primarily in the region $\{(V,a) : H(V,a) \geq 0, -2 \leq a \leq 2, 1 \leq V \leq 132\}$ which corresponds to positive acceleration and medium to high vehicle speeds, reflecting the increased energy demand under intense engine load. The area of increased emissions $\{(V,a) : H(V,a) < 0, -2 \leq a \leq 2, 1 \leq V \leq 132\}$ is continuous and extends from approximately 35–40 km/h upwards, encompassing a wide range of positive accelerations. In contrast, at low speeds, negative accelerations, and in the very low load zone, areas where CO_2 emissions for E85 are lower than for E10 are observed. This suggests that the differences between the fuels are primarily determined by driving dynamics, rather than just average emissions.

The boundary between the red and light-blue regions reveals how strongly the relative CO_2 performance of E85 depends on load intensity. When the driver demands rapid acceleration at medium and high speeds, the engine operates at high torque and E85 requires a larger injected fuel mass due to its lower heating value. Under these conditions, any efficiency benefits of ethanol are outweighed by the additional carbon released from the extra

fuel, which explains the compact but clearly defined red belt. Below this belt, in the large low- and medium-load domain, the map is dominated by the light-blue area, indicating that most everyday manoeuvres—gentle acceleration, cruising and deceleration—do not lead to higher CO_2 emissions with E85 and can even slightly reduce them compared with E10. This pattern implies that the real impact of switching to E85 will be strongly influenced by driving style and traffic conditions. Fleets or drivers characterised by frequent hard accelerations at higher speeds will experience a more pronounced CO_2 penalty, whereas smoother driving in urban and suburban contexts will largely neutralise, or partially reverse, this effect.

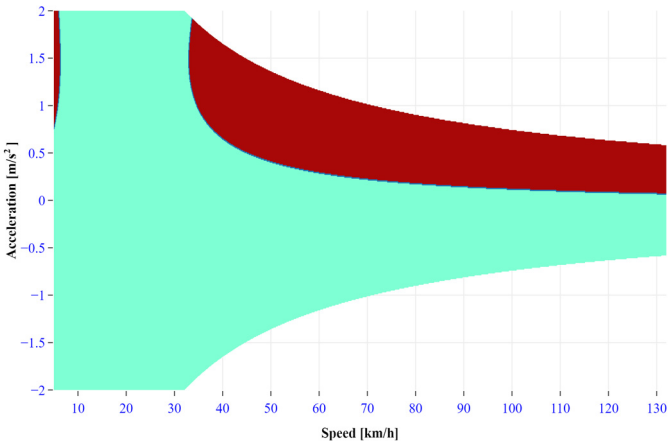

Figure 6. Regions of increased (red) and decreased (cyan) predicted CO_2 emissions for E85 relative to E10 in the speed–acceleration domain.

The discussed results cover a single vehicle and a single test environment, which naturally limits their generalizability. Therefore, the presented findings should be interpreted as vehicle- and test-specific and not directly extrapolated to other flex-fuel vehicles or real-world traffic conditions without further validation. Engine design differences, different operating conditions (highways, urban traffic, winter conditions), and the lack of parallel assessment of other exhaust gas components may influence the observed trends. Future research directions should include the analysis of a larger number of vehicles, various traffic scenarios, simultaneous assessment of CO_2 and regulated compounds, and integration of the proposed emission maps with fleet and city models.

6. Discussion

The obtained results confirm that the impact of E10 and E85 fuels on CO_2 emissions is not a simple function of the bioethanol content in the fuel, but rather depends significantly on the vehicle's operating state, described by speed and acceleration. Using emission maps in the speed-acceleration space and a differential index comparing E85 versus E10, it was demonstrated that the differences between the fuels are localised and appear in specific areas of this space, rather than as a uniform shift in emissions levels throughout the cycle.

The differences observed between E10 and E85 should be interpreted in the context of fuel physicochemical properties. E85 is characterised by a significantly higher octane rating (typically above RON 105) compared to E10 (RON ≈ 95), which enables knock-resistant operation. At the same time, E85 exhibits a substantially lower heating value (approximately 27 MJ/kg) than gasoline-dominant blends (≈42–43 MJ/kg) [91]. Under dynamic, high-load conditions, such as strong positive acceleration, the lower energy density of E85 requires a higher fuel mass flow to deliver comparable engine power. As the vehicle was operated with a production engine control strategy, the potential efficiency benefits associated with a higher octane rating were insufficient to offset the increased fuel

demand, which explains the higher instantaneous CO_2 emissions observed for E85 in the high-load regions of the speed–acceleration domain.

In the literature, laboratory and on-road studies indicate slight differences in CO_2 emissions for E85 compared to gasoline or low-ethanol blends (E5–E10). Many publications report a reduction in CO_2 emissions compared to conventional fuels of several to a dozen or so per cent, and some authors find no significant statistical differences in the values recorded from the exhaust system [2,84]. At the same time, well-to-wheel and LCAs emphasise that the main advantage of E85 relates to the greenhouse gas balance throughout the fuel's life cycle, not necessarily to lower CO_2 emissions during the combustion process itself [5,9]. The emission maps developed in this study for E10 and E85 fuels are consistent with these observations.

For most driving trajectories, the differences in instantaneous CO_2 emissions between fuels remain small.

What proves crucial is the speed and acceleration states the vehicle spends time at, and therefore, the load ranges in which the engine operates.

The obtained results confirm that E85 does not result in a uniform, constant reduction in CO_2 emissions throughout the entire driving cycle. Instead, it changes the emission structure in the engine operating state space, which is consistent with previous analyses of the effect of ethanol on combustion efficiency and fuel consumption [1,92,93], but here presented thanks to speed-acceleration maps. The literature emphasizes that speed and acceleration are among the most critical predictors of CO_2 emissions, with the highest emission values observed during positive accelerations and driving at higher speeds [36,82]. Speed- and acceleration-based CO_2 emission models, including those using VSP and machine learning methods, demonstrate very high predictive accuracy, emphasising the importance of acceleration and load-related trajectory sections [28,33,44].

The results of this study extend previous analyses because:

- They show that an identical trajectory (i.e., the same speed and acceleration curve) can generate different CO_2 emissions depending on the fuel type used,
- They indicate that the most significant differences between E10 and E85 are concentrated in the regions (v, a) corresponding to high acceleration and increased engine load.

Literature suggests that higher ethanol percentages may promote more complete combustion and reduce CO and HC emissions, while slightly increasing CO_2 emissions under certain operating conditions [1,85,92]. In turn, the lower calorific value of E85 leads to increased fuel consumption under high power demand conditions [2]. The difference map (Figure 6) well reflects this relationship:

- In the speed-acceleration region, instantaneous CO_2 emissions are lower for E85 than for E10 (due to the different elemental composition of ethanol, including its nominally higher H/C ratio but lower effective energy density resulting from the presence of oxygen in the molecule, which reduces the useful energy available during combustion).
- However, in higher load zones, these benefits are weakened or reversed due to the need to supply a larger fuel dose.

Thus, the presented approach enables us to transition from the classic question of "does E85 emit less CO_2 than E10?" to a more precise one: "in what parts of the driving cycle does E85 reduce CO_2 emissions, and in what parts does it increase them?" Such analyses are rarely found in the literature, which most often reports results in the form of average cycle values or emissions for selected operating points.

The introduction of the WLTP procedure led to an increase in reported CO_2 emissions compared to the NEDC, averaging 21–25% for passenger cars and approximately 27% for

commercial vehicles [15,16]. This is due to the more dynamic nature of the cycle, higher vehicle load, and more precise representation of acceleration and braking phases [94,95]. Real-world emissions studies further confirm that aggressive driving and intense acceleration can increase CO_2 emissions by several to a dozen or so percent compared to smooth driving [32].

The results obtained in this study are consistent with these observations:

- CO_2 emission maps clearly identify areas of the most significant emission increase during positive accelerations.
- Differences between E10 and E85 are primarily visible in these areas.
- However, during steady-state driving and during low accelerations, the impact of fuel type on instantaneous CO_2 emissions is significantly smaller.

From the perspective of fleet and regulatory models (COPERT, microscopic and structural models), this means that the CO_2 emission reduction potential of fuels with higher ethanol content depends on the structure of the vehicle's operating states. In low-dynamic cycles, the differences between E10 and E85 may be negligible; however, in urban conditions, especially for heavier vehicles, they can have a significant impact on final emissions [21,63].

In recent years, models of instantaneous CO_2 emissions based on speed, acceleration, VSP, and engine parameters have been intensively developed, employing statistical and machine learning methods. Many of them achieve very high predictive accuracy, especially when using data from OBD or PEMS [30,33,83]. In the presented work, a simplified regression approach was employed, focusing on model interpretability and the ability to determine the difference index across the entire (v, a) space. This solution complements more advanced ML methods, enabling direct representation of differences between fuels in the context of vehicle operating states.

The present study deliberately focuses on CO_2 emissions, as they are directly linked to vehicle energy demand, engine load, and driving dynamics. Other regulated exhaust components associated with ethanol fuels (e.g., NO_x, aldehydes, unburned ethanol) are governed by different formation mechanisms and may respond differently to load and combustion conditions; therefore, they are not analysed in detail here and are addressed in separate, dedicated studies. It should be emphasised that the presented analysis concerns only exhaust emissions. From a climate perspective, the origin of carbon in the fuel is also crucial. Bioethanol can reduce greenhouse gas emissions by up to 40–70% compared to gasoline, depending on the feedstock and process parameters [9]. However, caution is needed when assessing the "carbon neutrality" of first-generation ethanol due to possible land-use changes and methodological uncertainties [69]. In light of these data, the presented results can be interpreted in two ways:

- At the tailpipe emission level, as the differences between E10 and E85 are limited and dependent on the load structure.
- At the life cycle level, where E85 may be a more climate-favourable fuel, provided appropriate raw materials and production technology are used [79].

The discussed results cover a single vehicle and a single test environment, which naturally limits their generalizability. Engine design differences, different operating conditions (highways, urban traffic, winter conditions), and the lack of parallel assessment of other exhaust gas components may influence the observed trends. Future research directions should include the analysis of a larger number of vehicles, various traffic scenarios, simultaneous assessment of CO_2 and regulated compounds, and integration of the proposed emission maps with fleet and city models.

7. Conclusions

This study investigated dynamic CO_2 emission differences between E10 and E85 fuels using speed-acceleration-based emission mapping under WLTP conditions. The main novel contributions and key findings of the study can be summarised as follows:

- The study proposes a speed–acceleration-based framework for comparing instantaneous CO_2 emissions between fuels, moving beyond conventional cycle-averaged indicators.
- Emission surfaces and a differential index were used to identify localised regions in the operating state space where fuel-dependent differences occur, rather than assuming uniform emission shifts.
- The results demonstrate that E85 does not lead to a consistent reduction in instantaneous CO_2 emissions across the entire WLTP cycle, but alters the emission structure depending on vehicle load and acceleration.
- The most significant differences between E10 and E85 were observed in regions associated with high positive acceleration and increased engine load, where E85 tended to exhibit higher instantaneous CO_2 emissions.
- Under steady-state and low-acceleration conditions, the differences in instantaneous CO_2 emissions between the two fuels were limited.
- The proposed approach provides a transparent and interpretable alternative to more complex emission models, with potential applicability in fleet, regulatory, and traffic emission assessments.

This study analysed CO_2 emissions generated by a flex-fuel vehicle during the WLTP test, fuelled successively with E10 and E85 fuels. Using a single vehicle and identical test conditions allowed for the unambiguous attribution of observed differences to fuel composition. The recorded data were used to develop speed- and acceleration-dependent instantaneous emission models and to determine the emission surface in space (v, a), enabling a comprehensive characterisation of dynamic emission changes during the cycle.

The results indicate that CO_2 emissions for both fuels are strongly dependent on driving dynamics. The highest emission values occur during positive accelerations at medium and high speeds, confirming the dominant role of engine load in generating instantaneous emission peaks. E85 fuel is characterised by more pronounced emission peaks in these areas, a direct consequence of its lower calorific value and increased fuel consumption under conditions of high-power demand. During steady state driving and at low loads, the differences between E10 and E85 are reduced, and in some cases, even reversed.

Using the differential index $H(V, a)$ allowed for the detailed identification of areas where E85 generates higher or lower CO_2 emissions compared to E10. These results clearly demonstrate that the fuel effect is not uniform and results primarily from the operating states that dominate the driving cycle. This approach provides a much more comprehensive picture than traditional comparisons based on average values. It is emphasised that fuel properties are revealed in a non-linear manner depending on load characteristics.

More broadly, the results confirm existing literature observations that exhaust CO_2 emissions from E85 can be comparable to or slightly higher than those of E10. At the same time, significant climate benefits only become apparent after considering the carbon source and a comprehensive fuel life cycle analysis. The presented approach, based on emission maps as a function of speed and acceleration, provides a practical tool for further study, including optimisation of control strategies, assessment of driving style effects, and integration with fleet emission models.

The conducted research shows that comparing ethanol and conventional fuels requires high-resolution analysis, not only at the level of average emissions but also across the entire range of engine operating conditions. These results can serve as a starting point for more advanced studies involving a larger number of vehicles, RDE conditions, and

the simultaneous assessment of other exhaust gas components, particularly compounds specific to ethanol fuels.

Author Contributions: Conceptualization, P.L., E.K., M.Z.-L. and J.M.; methodology, P.L., E.K. and M.Z.-L.; software, E.K., validation, P.L., E.K., M.Z.-L., P.W. and J.M.; formal analysis, P.L., E.K., M.Z.-L. and J.M.; investigation, P.L., M.Z.-L., P.W., J.M., M.K.W., R.K. and S.D.; resources, P.L., M.Z.-L., P.W., J.M., S.O., M.K.W., R.K. and S.D.; data curation, P.L., M.Z.-L., P.W. and J.M.; writing—original draft preparation, M.Z.-L.; writing—review and editing, P.L., E.K., M.Z.-L., P.W., J.M., M.K.W., R.K. and S.D.; visualization, P.L., M.Z.-L. and J.M.; supervision, P.L., E.K. and S.O.; project administration, P.L.; funding acquisition, P.L., E.K. and J.M. All authors have read and agreed to the published version of the manuscript.

Funding: This research received no external funding.

Data Availability Statement: The original contributions presented in this study are included in the article. Further inquiries can be directed to the corresponding author.

Acknowledgments: The experimental campaign was conducted at the Environment Protection Centre of the Motor Transport Institute (ITS). The special equipment used in the study was purchased with funds from the IMECH project under the same programme. Research was funded by Warsaw University of Technology within the Excellence Initiative: Research University (IDUB) programme.

Conflicts of Interest: The authors declare no conflict of interest.

Abbreviations

The following abbreviations are used in this manuscript:

AFR	Air–Fuel Ratio
AI	Artificial Intelligence
BECCS	Bioenergy with Carbon Capture and Storage
CCS	Carbon Capture and Storage
COPERT	COmputer Programme to calculate Emissions from Road Transport
E10	Gasoline with 10% ethanol
E85	Ethanol fuel blend containing 85% ethanol and 15% gasoline
FFV	Flex-Fuel Vehicle
GHG	Greenhouse Gases
IoT	Internet of Things
LCA	Life Cycle Assessment
LSTM	Long Short-Term Memory
MLP	Multilayer Perceptron
NEDC	New European Driving Cycle
OBD	On-Board Diagnostics
PEMS	Portable Emissions Measurement System
RDE	Real Driving Emissions
SHAP	SHapley Additive exPlanations
SI engine	Spark-Ignition engine
VSP	Vehicle Specific Power
WLTC	Worldwide Harmonized Light-Duty Test Cycle
WLTP	Worldwide Harmonized Light Vehicles Test Procedure

References

1. Tibaquirá, J.; Huertas, J.; Ospina, S.; Quirama, L.; Niño, J. The Effect of Using Ethanol-Gasoline Blends on the Mechanical, Energy and Environmental Performance of In-Use Vehicles. *Energies* **2018**, *11*, 221. [CrossRef]
2. Myung, C.-L.; Choi, K.; Cho, J.; Kim, K.; Baek, S.; Lim, Y.; Park, S. Evaluation of Regulated, Particulate, and BTEX Emissions Inventories from a Gasoline Direct Injection Passenger Car with Various Ethanol Blended Fuels under Urban and Rural Driving Cycles in Korea. *Fuel* **2020**, *262*, 116406. [CrossRef]

3. Frutuoso, F.S.; Alves, C.M.A.C.; Araújo, S.L.; Serra, D.S.; Barros, A.L.B.P.; Cavalcante, F.S.Á.; Araújo, R.S.; Policarpo, N.A.; Oliveira, M.L.M. Assessing Light Flex-Fuel Vehicle Emissions with Ethanol/Gasoline Blends along an Urban Corridor: A Case of Fortaleza/Brazil. *Int. J. Transp. Sci. Technol.* **2023**, *12*, 447–459. [CrossRef]
4. Warguła, Ł.; Wieczorek, B.; Gierz, Ł.; Karwat, B. Critical Concerns Regarding the Transition from E5 to E10 Gasoline in the European Union, Particularly in Poland in 2024—A Theoretical and Experimental Analysis of the Problem of Controlling the Air–Fuel Mixture Composition (AFR) and the λ Coefficient. *Energies* **2025**, *18*, 852. [CrossRef]
5. Novakovic, M.; Tuner, M.; Garcia, A.; Verhelst, S. An Experimental Investigation of Directly Injected E85 Fuel in a Heavy-Duty Compression Ignition Engine. In Proceedings of the SAE Powertrains, Fuels & Lubricants Conference & Exhibition, Krakow, Poland, 6–8 September 2022.
6. Gupta, S.; Kanchan, S.; Kaur, R.; Sandhu, S.S. Investigation of Performance and Emission Characteristics Using Ethanol-Blended Gasoline Fuel as a Flex-Fuel in Two-Wheeler Vehicle Mounted on a Chassis Dynamometer. *Clean. Energy* **2024**, *8*, 174–193. [CrossRef]
7. Rimkus, A.; Pukalskas, S.; Mejeras, G.; Nagurnas, S. Impact of Bioethanol Concentration in Gasoline on SI Engine Sustainability. *Sustainability* **2024**, *16*, 2397. [CrossRef]
8. Mateo, N.E.R.; Calderon, A.; Agrupis, S.; Manzano, L.F.T.; Baga, C.C.; Fagaragan, A. Nipa-Based Bioethanol as a Renewable Pure Engine Fuel: A Preliminary Performance Testing and Carbon Footprint Quantification. *Int. J. Renew. Energy Dev.* **2025**, *14*, 39–51. [CrossRef]
9. Daylan, B.; Ciliz, N. Life Cycle Assessment and Environmental Life Cycle Costing Analysis of Lignocellulosic Bioethanol as an Alternative Transportation Fuel. *Renew. Energy* **2016**, *89*, 578–587. [CrossRef]
10. Ghani, H.U.; Gheewala, S.H. Environmental Sustainability Assessment of Molasses-Based Bioethanol Fuel in Pakistan. *Sustain. Prod. Consum.* **2021**, *27*, 402–410. [CrossRef]
11. Policarpo, N.A.; Frutuoso, F.S.; Cassiano, D.R.; Cavalcante, F.S.A.; Araújo, R.S.; Bertoncini, B.V.; Oliveira, M.L.M. Emission Estimates for an On-Road Flex-Fuel Vehicles Operated by Ethanol-Gasoline Blends in an Urban Region, Brazil. *Urban. Clim.* **2018**, *24*, 111–120. [CrossRef]
12. Songkitti, W.; Aroonsrisopon, T.; Wirojsakunchai, E. An Analysis of Emissions from An Ethanol Flex-Fuel Vehicle under Two Distinct Driving Cycle Tests during Cold Start. *Int. J. Automot. Mech. Eng.* **2022**, *19*, 9551–9562. [CrossRef]
13. De Salvo Junior, O.; Silva Forcetto, A.L.; Maria Laganá, A.A.; Vaz De Almeida, F.G.; Baptista, P. Combining On-Road Measurements and Life-Cycle Carbon Emissions of Flex-Fuel Vehicle. *Renew. Sustain. Energy Rev.* **2024**, *204*, 114784. [CrossRef]
14. Santos, A.S.; Gilio, L.; Halmenschlager, V.; Diniz, T.B.; Almeida, A.N. Flexible-Fuel Automobiles and CO 2 Emissions in Brazil: Parametric and Semiparametric Analysis Using Panel Data. *Habitat. Int.* **2018**, *71*, 147–155. [CrossRef]
15. Pavlovic, J.; Ciuffo, B.; Fontaras, G.; Valverde, V.; Marotta, A. How Much Difference in Type-Approval CO_2 Emissions from Passenger Cars in Europe Can Be Expected from Changing to the New Test Procedure (NEDC vs. WLTP)? *Transp. Res. Part A Policy Pract.* **2018**, *111*, 136–147. [CrossRef]
16. Chatzipanagi, A.; Pavlovic, J.; Ktistakis, M.A.; Komnos, D.; Fontaras, G. Evolution of European Light-Duty Vehicle CO_2 Emissions Based on Recent Certification Datasets. *Transp. Res. Part D Transp. Environ.* **2022**, *107*, 103287. [CrossRef] [PubMed]
17. Jaworski, A.; Mądziel, M.; Lew, K.; Campisi, T.; Woś, P.; Kuszewski, H.; Wojewoda, P.; Ustrzycki, A.; Balawender, K.; Jakubowski, M. Evaluation of the Effect of Chassis Dynamometer Load Setting on CO_2 Emissions and Energy Demand of a Full Hybrid Vehicle. *Energies* **2021**, *15*, 122. [CrossRef]
18. Fortune, J.-F.; Cologon, P.; Hayrault, P.; Heninger, M.; Leprovost, J.; Lemaire, J.; Anselmi, P.; Matrat, M. Impact of Fuel Ethanol Content on Regulated and Non-Regulated Emissions Monitored by Various Analytical Techniques over Flex-Fuel and Conversion Kit Applications. *Fuel* **2023**, *334*, 126669. [CrossRef]
19. Di Iorio, S.; Catapano, F.; Magno, A.; Sementa, P.; Vaglieco, B.M. The Potential of Ethanol/Methanol Blends as Renewable Fuels for DI SI Engines. *Energies* **2023**, *16*, 2791. [CrossRef]
20. Laskowski, P.; Zimakowska-Laskowska, M. Simulation Study of the Effect of Ethanol Content in Fuel on Petrol Engine Performance and Exhaust Emissions. *Combust. Engines* **2025**, *201*, 129–135. [CrossRef]
21. Triantafyllopoulos, G.; Dimaratos, A.; Ntziachristos, L.; Bernard, Y.; Dornoff, J.; Samaras, Z. A Study on the CO_2 and NOx Emissions Performance of Euro 6 Diesel Vehicles under Various Chassis Dynamometer and On-Road Conditions Including Latest Regulatory Provisions. *Sci. Total Environ.* **2019**, *666*, 337–346. [CrossRef]
22. Liu, Y.; Martinet, S.; Louis, C.; Pasquier, A.; Tassel, P.; Perret, P. Emission Characterization of In-Use Diesel and Gasoline Euro 4 to Euro 6 Passenger Cars Tested on Chassis Dynamometer Bench and Emission Model Assessment. *Aerosol Air Qual. Res.* **2017**, *17*, 2289–2299. [CrossRef]
23. Zimakowska-Laskowska, M.; Kozłowski, E.; Laskowski, P.; Wiśniowski, P.; Świderski, A.; Orynycz, O. Vehicle Exhaust Emissions in the Light of Modern Research Tools: Synergy of Chassis Dynamometers and Computational Models. *Combust. Engines* **2025**, *200*, 145–154. [CrossRef]

24. Dimaratos, A.; Toumasatos, Z.; Doulgeris, S.; Triantafyllopoulos, G.; Kontses, A.; Samaras, Z. Assessment of CO_2 and NOx Emissions of One Diesel and One Bi-Fuel Gasoline/CNG Euro 6 Vehicles During Real-World Driving and Laboratory Testing. *Front. Mech. Eng.* **2019**, *5*, 62. [CrossRef]
25. Kozłowski, E.; Rimkus, A.; Zimakowska-Laskowska, M.; Matijošius, J.; Wiśniowski, P.; Traczyński, M.; Laskowski, P.; Madlenak, R. Energy and Environmental Impacts of Replacing Gasoline with LPG Under Real Driving Conditions. *Energies* **2025**, *18*, 5522. [CrossRef]
26. Kuranc, A.; Caban, J.; Šarkan, B.; Dudziak, A.; Stoma, M. Emission of Selected Exhaust Gas Components and Fuel Consumption in Different Driving Cycles. *Komunikácie* **2021**, *23*, B265–B277. [CrossRef]
27. Mogno, C.; Fontaras, G.; Arcidiacono, V.; Komnos, D.; Pavlovic, J.; Ciuffo, B.; Makridis, M.; Valverde, V. The Application of the CO2MPAS Model for Vehicle CO_2 Emissions Estimation over Real Traffic Conditions. *Transp. Policy* **2022**, *124*, 152–159. [CrossRef]
28. Orynycz, O.; Zimakowska-Laskowska, M.; Kulesza, E. CO_2 Emission and Energy Consumption Estimates in the COPERT Model—Conclusions from Chassis Dynamometer Tests and SANN Artificial Neural Network Models and Their Meaning for Transport Management. *Energies* **2025**, *18*, 3457. [CrossRef]
29. Li, S.; Tong, Z.; Haroon, M. Estimation of Transport CO_2 Emissions Using Machine Learning Algorithm. *Transp. Res. Part. D Transp. Environ.* **2024**, *133*, 104276. [CrossRef]
30. Zhang, Q.; Wei, N.; Mao, H. Impact of Ethanol-Gasoline Implementation on Vehicle Emission Based on Remote Sensing Test. *Environ. Res. Commun.* **2022**, *4*, 055008. [CrossRef]
31. Dong, Y.; Xu, J.; Ni, J. Carbon Emission Model of Vehicles Driving at Fluctuating Speed on Highway. *Environ. Sci. Pollut. Res.* **2022**, *30*, 18064–18077. [CrossRef] [PubMed]
32. Suarez, J.; Makridis, M.; Anesiadou, A.; Komnos, D.; Ciuffo, B.; Fontaras, G. Benchmarking the Driver Acceleration Impact on Vehicle Energy Consumption and CO_2 Emissions. *Transp. Res. Part D Transp. Environ.* **2022**, *107*, 103282. [CrossRef] [PubMed]
33. Alam, G.M.I.; Arfin Tanim, S.; Sarker, S.K.; Watanobe, Y.; Islam, R.; Mridha, M.F.; Nur, K. Deep Learning Model Based Prediction of Vehicle CO_2 Emissions with eXplainable AI Integration for Sustainable Environment. *Sci. Rep.* **2025**, *15*, 3655. [CrossRef] [PubMed]
34. Khajavi, H.; Rastgoo, A. Predicting the Carbon Dioxide Emission Caused by Road Transport Using a Random Forest (RF) Model Combined by Meta-Heuristic Algorithms. *Sustain. Cities Soc.* **2023**, *93*, 104503. [CrossRef]
35. Zhaparova, S.; Kulisz, M.; Kospanov, N.; Ibrayeva, A.; Bayazitova, Z.; Kurmanbayeva, A. Modeling Air Pollution from Urban Transport and Strategies for Transitioning to Eco-Friendly Mobility in Urban Environments. *Environments* **2025**, *12*, 411. [CrossRef]
36. Le Cornec, C.M.A.; Molden, N.; Van Reeuwijk, M.; Stettler, M.E.J. Modelling of Instantaneous Emissions from Diesel Vehicles with a Special Focus on NOx: Insights from Machine Learning Techniques. *Sci. Total Environ.* **2020**, *737*, 139625. [CrossRef]
37. Wang, Y.; Lin, C.; Zhao, B.; Gong, B.; Liu, H. Trajectory-Based Vehicle Emission Evaluation for Signalized Intersection Using Roadside LiDAR Data. *J. Clean. Prod.* **2024**, *440*, 140971. [CrossRef]
38. Zhai, Z.; Tu, R.; Xu, J.; Wang, A.; Hatzopoulou, M. Capturing the Variability in Instantaneous Vehicle Emissions Based on Field Test Data. *Atmosphere* **2020**, *11*, 765. [CrossRef]
39. Mądziel, M. Instantaneous CO_2 Emission Modelling for a Euro 6 Start-Stop Vehicle Based on Portable Emission Measurement System Data and Artificial Intelligence Methods. *Environ. Sci. Pollut. Res.* **2023**, *31*, 6944–6959. [CrossRef]
40. Jang, S.; Song, K.-H.; Kim, D.; Ko, J.; Lee, S.M.; Elkosantini, S.; Suh, W. Road-Section-Based Analysis of Vehicle Emissions and Energy Consumption. *Sustainability* **2023**, *15*, 4421. [CrossRef]
41. Zhong, H.; Chen, K.; Liu, C.; Zhu, M.; Ke, R. Models for Predicting Vehicle Emissions: A Comprehensive Review. *Sci. Total Environ.* **2024**, *923*, 171324. [CrossRef]
42. Wu, F.; Zhu, J.; Yang, H.; He, X.; Peng, Q. Data-Driven Symmetry and Asymmetry Investigation of Vehicle Emissions Using Machine Learning: A Case Study in Spain. *Symmetry* **2025**, *17*, 1223. [CrossRef]
43. Ramirez-Sanchez, E.; Tang, C.; Xu, Y.; Renganathan, N.; Jayawardana, V.; He, Z.; Wu, C. NeuralMOVES: A Lightweight and Microscopic Vehicle Emission Estimation Model Based on Reverse Engineering and Surrogate Learning. *arXiv* **2025**, arXiv:2502.04417. [CrossRef]
44. Ahmed, O.; Ramadan, I.; Shawky, M. Modelling Vehicle Emissions and Fuel Consumption Based on Instantaneous Speed and Acceleration Levels. *Eng. Res. J. Fac. Eng.* **2022**, *51*, 106–116. [CrossRef]
45. Volintiru, O.N.; Mărășescu, D.; Coșofreț, D.; Popa, A. Aspects Regarding the CO_2 Footprint Developed by Marine Diesel Engines. *Fire* **2025**, *8*, 240. [CrossRef]
46. Mohassab, H.; Abouelsoud, M.; Shmroukh, A.N.; Ghazaly, N.M. Experimental Investigation of Performance, Combustion Efficiency and Emissions of SI Engine for Several Octane Numbers. *J. Adv. Res. Fluid. Mech. Therm. Sc.* **2025**, *127*, 81–105. [CrossRef]
47. Wang, J.; Dai, H.; Feng, H.; Guo, M.; Zylianov, V.; Feng, Z.; Cui, J. Carbon Emission of Urban Vehicles Based on Carbon Emission Factor Correlation Analysis. *Sci. Rep.* **2025**, *15*, 2037. [CrossRef]

48. Longo, K.; Wang, X.; Zhao, H. Impact of Diesel-Hythane Dual-Fuel Combustion on Engine Performance and Emissions in a Heavy-Duty Engine at Low-Load Condition. *Int. J. Engine Res.* **2024**, *25*, 276–292. [CrossRef]
49. Chen, Y.; Zhang, J.; Zhang, Z.; Zhang, B.; Hu, J.; Zhong, W.; Ye, Y. Effect of Ammonia Energy Ratio and Load on Combustion and Emissions of an Ammonia/Diesel Dual-Fuel Engine. *Energy* **2024**, *302*, 131860. [CrossRef]
50. Chojnowski, J.; Karczewski, M.; Szamrej, G.A. Dual-Fuel Engines Using Hydrogen-Enriched Fuels as an Ecological Source of Energy for Transport, Industry and Power Engineering. *Combust. Engines* **2024**, *198*, 3–12. [CrossRef]
51. Rimkus, A.; Kozłowski, E.; Vipartas, T.; Pukalskas, S.; Wiśniowski, P.; Matijošius, J. Emission Characteristics of Hydrogen-Enriched Gasoline Under Dynamic Driving Conditions. *Energies* **2025**, *18*, 1190. [CrossRef]
52. Subramanian, T.; Varuvel, E.G.; Leenus, J.M.; Beddhannan, N. Effect of Electrochemical Conversion of Biofuels Using Ionization System on CO_2 Emission Mitigation in CI Engine along with Post-Combustion System. *Fuel Process. Technol.* **2018**, *173*, 21–29. [CrossRef]
53. Wasilewski, J.; Szyszlak-Bargłowicz, J.; Zając, G.; Szczepanik, M. Assessment of Co_2 Emission by Tractor Engine at Varied Control Settings of Fuel Unit. *Agric. Eng.* **2020**, *24*, 105–115. [CrossRef]
54. Dižo, J.; Blatnický, M.; Sága, M.; Šťastniak, P. A Numerical Study of a Compressed Air Engine with Rotating Cylinders. *Appl. Sci.* **2021**, *11*, 7504. [CrossRef]
55. Cristofanelli, P.; Fratticioli, C.; Hazan, L.; Chariot, M.; Couret, C.; Gazetas, O.; Kubistin, D.; Laitinen, A.; Leskinen, A.; Laurila, T.; et al. Identification of Spikes in Continuous Ground-Based in Situ Time Series of CO_2, CH_4 and CO: An Extended Experiment within the European ICOS Atmosphere Network. *Atmos. Meas. Tech.* **2023**, *16*, 5977–5994. [CrossRef]
56. El Yazidi, A.; Ramonet, M.; Ciais, P.; Broquet, G.; Pison, I.; Abbaris, A.; Brunner, D.; Conil, S.; Delmotte, M.; Gheusi, F.; et al. Identification of Spikes Associated with Local Sources in Continuous Time Series of Atmospheric CO, CO_2 and CH_4. *Atmos. Meas. Tech.* **2018**, *11*, 1599–1614. [CrossRef]
57. Ryoo, J.-M.; Fung, I.; Ehleringer, J.R. Short-Term Energy and Meteorological Impacts on Thanksgiving CO_2 in Salt Lake City. *Environ. Res. Commun.* **2025**, *7*, 065001. [CrossRef]
58. Mądziel, M.; Jaworski, A.; Kuszewski, H.; Woś, P.; Campisi, T.; Lew, K. The Development of CO_2 Instantaneous Emission Model of Full Hybrid Vehicle with the Use of Machine Learning Techniques. *Energies* **2021**, *15*, 142. [CrossRef]
59. Ajala, A.A.; Adeoye, O.L.; Salami, O.M.; Jimoh, A.Y. An Examination of Daily CO_2 Emissions Prediction through a Comparative Analysis of Machine Learning, Deep Learning, and Statistical Models. *Environ. Sci. Pollut. Res.* **2025**, *32*, 2510–2535. [CrossRef] [PubMed]
60. Singh, M.; Dubey, R. Deep Learning Model Based CO_2 Emissions Prediction Using Vehicle Telematics Sensors Data. *IEEE Trans. Intell. Veh.* **2023**, *8*, 768–777. [CrossRef]
61. Zhang, Y.; Zhou, R.; Peng, S.; Mao, H.; Yang, Z.; Andre, M.; Zhang, X. Development of Vehicle Emission Model Based on Real-Road Test and Driving Conditions in Tianjin, China. *Atmosphere* **2022**, *13*, 595. [CrossRef]
62. Rosero, F.; Rosero, C.X.; Segovia, C. Towards Simpler Approaches for Assessing Fuel Efficiency and CO_2 Emissions of Vehicle Engines in Real Traffic Conditions Using On-Board Diagnostic Data. *Energies* **2024**, *17*, 4814. [CrossRef]
63. Fontaras, G.; Ciuffo, B.; Zacharof, N.; Tsiakmakis, S.; Marotta, A.; Pavlovic, J.; Anagnostopoulos, K. The Difference between Reported and Real-World CO_2 Emissions: How Much Improvement Can Be Expected by WLTP Introduction? *Transp. Res. Procedia* **2017**, *25*, 3933–3943. [CrossRef]
64. Hasan Shahariar, G.M.; Sajjad, M.; Suara, K.A.; Jahirul, M.I.; Chu-Van, T.; Ristovski, Z.; Brown, R.J.; Bodisco, T.A. On-Road CO_2 and NOx Emissions of a Diesel Vehicle in Urban Traffic. *Transp. Res. Part D Transp. Environ.* **2022**, *107*, 103326. [CrossRef]
65. Qi, Z.; Gu, M.; Cao, J.; Zhang, Z.; You, C.; Zhan, Y.; Ma, Z.; Huang, W. The Effects of Varying Altitudes on the Rates of Emissions from Diesel and Gasoline Vehicles Using a Portable Emission Measurement System. *Atmosphere* **2023**, *14*, 1739. [CrossRef]
66. Jiang, Z.; Wu, L.; Niu, H.; Jia, Z.; Qi, Z.; Liu, Y.; Zhang, Q.; Wang, T.; Peng, J.; Mao, H. Investigating the Impact of High-Altitude on Vehicle Carbon Emissions: A Comprehensive on-Road Driving Study. *Sci. Total Environ.* **2024**, *918*, 170671. [CrossRef]
67. García, A.; Monsalve-Serrano, J.; Martínez-Boggio, S.; Rückert Roso, V.; Duarte Souza Alvarenga Santos, N. Potential of Bio-Ethanol in Different Advanced Combustion Modes for Hybrid Passenger Vehicles. *Renew. Energy* **2020**, *150*, 58–77. [CrossRef]
68. Ogunkunle, O.; Ahmed, N.A. Overview of Biodiesel Combustion in Mitigating the Adverse Impacts of Engine Emissions on the Sustainable Human–Environment Scenario. *Sustainability* **2021**, *13*, 5465. [CrossRef]
69. DeCicco, J.M.; Liu, D.Y.; Heo, J.; Krishnan, R.; Kurthen, A.; Wang, L. Carbon Balance Effects of U.S. Biofuel Production and Use. *Clim. Change* **2016**, *138*, 667–680. [CrossRef]
70. Jaspers, B.C.; Kuo, P.-C.; Amladi, A.; Van Neerbos, W.; Aravind, P.V. Negative CO_2 Emissions for Transportation. *Front. Energy Res.* **2021**, *9*, 626538. [CrossRef]
71. Wiltink, T.; Ramirez Ramirez, A.; Pérez-Fortes, M. Trade-Offs in the Integration of Biogenic CO_2-Based Supply Chains for Storage and Use in the Transport Sector. In Proceedings of the 17th Greenhouse Gas Control Technologies Conference (GHGT-17), Calgary, AB, Canada, 20–24 October 2024. [CrossRef]

72. Christianides, D.; Bagaki, D.A.; Timmers, R.A.; Zrimec, M.B.; Theodoropoulou, A.; Angelidaki, I.; Kougias, P.; Zampieri, G.; Kamergi, N.; Napoli, A.; et al. Biogenic CO_2 Emissions in the EU Biofuel and Bioenergy Sector: Mapping Sources, Regional Trends, and Pathways for Capture and Utilisation. *Energies* **2025**, *18*, 1345. [CrossRef]
73. Labib, S.M.; Neema, M.N.; Rahaman, Z.; Patwary, S.H.; Shakil, S.H. Carbon Dioxide Emission and Bio-Capacity Indexing for Transportation Activities: A Methodological Development in Determining the Sustainability of Vehicular Transportation Systems. *J. Environ. Manag.* **2018**, *223*, 57–73. [CrossRef]
74. Bezyk, Y.; Sówka, I.; Górka, M. Assessment of Urban CO_2 Budget: Anthropogenic and Biogenic Inputs. *Urban. Clim.* **2021**, *39*, 100949. [CrossRef]
75. Kim, J.; Berelson, W.M.; Rollins, N.E.; Asimow, N.G.; Newman, C.; Cohen, R.C.; Miller, J.B.; McDonald, B.C.; Peischl, J.; Lehman, S.J. Observing Anthropogenic and Biogenic CO_2 Emissions in Los Angeles Using a Dense Sensor Network. *Environ. Sci. Technol.* **2025**, *59*, 3508–3517. [CrossRef] [PubMed]
76. Dees, J.; Oke, K.; Goldstein, H.; McCoy, S.T.; Sanchez, D.L.; Simon, A.J.; Li, W. Cost and Life Cycle Emissions of Ethanol Produced with an Oxyfuel Boiler and Carbon Capture and Storage. *Environ. Sci. Technol.* **2023**, *57*, 5391–5403. [CrossRef] [PubMed]
77. Brandão, M.; Heijungs, R.; Cowie, A.L. On Quantifying Sources of Uncertainty in the Carbon Footprint of Biofuels: Crop/Feedstock, LCA Modelling Approach, Land-Use Change, and GHG Metrics. *Biofuel Res. J.* **2022**, *9*, 1608–1616. [CrossRef]
78. Soleymani Angili, T.; Grzesik, K.; Rödl, A.; Kaltschmitt, M. Life Cycle Assessment of Bioethanol Production: A Review of Feedstock, Technology and Methodology. *Energies* **2021**, *14*, 2939. [CrossRef]
79. Umesh; Moholkar, V.S. 2G Bioethanol for Sustainable Transport Sector: Review and Analysis of the Life Cycle Assessments. *Curr. Pollut. Rep.* **2025**, *11*, 11. [CrossRef]
80. Osman, A.I.; Chen, L.; Yang, M.; Msigwa, G.; Farghali, M.; Fawzy, S.; Rooney, D.W.; Yap, P.-S. Cost, Environmental Impact, and Resilience of Renewable Energy under a Changing Climate: A Review. *Environ. Chem. Lett.* **2023**, *21*, 741–764. [CrossRef]
81. Rahman, A.; Murad, S.M.W.; Mohsin, A.K.M.; Wang, X. Does Renewable Energy Proactively Contribute to Mitigating Carbon Emissions in Major Fossil Fuels Consuming Countries? *J. Clean. Prod.* **2024**, *452*, 142113. [CrossRef]
82. Wang, Z.; Mae, M.; Nishimura, S.; Matsuhashi, R. Vehicular Fuel Consumption and CO_2 Emission Estimation Model Integrating Novel Driving Behavior Data Using Machine Learning. *Energies* **2024**, *17*, 1410. [CrossRef]
83. Seo, J.; Park, S. Optimizing Model Parameters of Artificial Neural Networks to Predict Vehicle Emissions. *Atmos. Environ.* **2023**, *294*, 119508. [CrossRef]
84. Tang, T.; McCaffery, C.; Ma, T.; Hao, P.; Durbin, T.D.; Johnson, K.C.; Karavalakis, G. Expanding the Ethanol Blend Wall in California: Emissions Comparison between E10 and E15. *Fuel* **2023**, *350*, 128836. [CrossRef]
85. Kozak, M.; Waligórski, M.; Wcisło, G.; Wierzbicki, S.; Duda, K. Exhaust Emissions from a Direct Injection Spark-Ignition Engine Fueled with High-Ethanol Gasoline. *Energies* **2025**, *18*, 454. [CrossRef]
86. Hunicz, J. *Modelowanie Silników Spalinowych (Modeling of Internal Combustion Engines)*; Lublin University of Technology Publishing House: Lublin, Poland, 2014.
87. Hastie, T.; Tibshirani, R.; Friedman, J. *The Elements of Statistical Learning*; Springer Series in Statistics; Springer: New York, NY, USA, 2009; ISBN 978-0-387-84857-0.
88. James, G.; Witten, D.; Hastie, T.; Tibshirani, R. *An Introduction to Statistical Learning: With Applications in R*; Springer Texts in Statistics; Springer: New York, NY, USA, 2021; ISBN 978-1-0716-1417-4.
89. Pawlik, P.; Kania, K.; Przysucha, B. Fault Diagnosis of Machines Operating in Variable Conditions Using Artificial Neural Network Not Requiring Training Data from a Faulty Machine. *Eksploat. I Niezawodn. Maint. Reliab.* **2023**, *25*, 168109. [CrossRef]
90. Kłosowski, G.; Rymarczyk, T.; Niderla, K.; Kulisz, M.; Skowron, Ł.; Soleimani, M. Using an LSTM Network to Monitor Industrial Reactors Using Electrical Capacitance and Impedance Tomography—A Hybrid Approach. *Eksploat. I Niezawodn. Maint. Reliab.* **2023**, *25*, 11. [CrossRef]
91. Tamam, M.Q.M.; Abdullah, N.R.; Yahya, W.J.; Kadir, H.A.; Putrasari, Y.; Ahmad, M.A. Effects of Ethanol Blending with Methanol-Gasoline Fuel on Spark Ignition Engine Performance and Emissions. *J. Adv. Res. Fluid Mech. Therm. Sci.* **2021**, *83*, 54–72. [CrossRef]
92. Doğan, B.; Erol, D.; Yaman, H.; Kodanli, E. The Effect of Ethanol-Gasoline Blends on Performance and Exhaust Emissions of a Spark Ignition Engine through Exergy Analysis. *Appl. Therm. Eng.* **2017**, *120*, 433–443. [CrossRef]
93. Pavlovic, J.; Marotta, A.; Ciuffo, B. CO_2 Emissions and Energy Demands of Vehicles Tested under the NEDC and the New WLTP Type Approval Test Procedures. *Appl. Energy* **2016**, *177*, 661–670. [CrossRef]

94. Tsokolis, D.; Tsiakmakis, S.; Dimaratos, A.; Fontaras, G.; Pistikopoulos, P.; Ciuffo, B.; Samaras, Z. Fuel Consumption and CO_2 Emissions of Passenger Cars over the New Worldwide Harmonized Test Protocol. *Appl. Energy* **2016**, *179*, 1152–1165. [CrossRef]
95. Shahariar, G.M.H.; Bodisco, T.A.; Zare, A.; Sajjad, M.; Jahirul, M.I.; Van, T.C.; Bartlett, H.; Ristovski, Z.; Brown, R.J. Impact of Driving Style and Traffic Condition on Emissions and Fuel Consumption During Real-World Transient Operation. *Fuel* **2022**, *319*, 123874. [CrossRef]